research papers

Evaluation of two methods to minimize the anticlastic curvature of cylindrical bent crystals

Liangjie Feng,* Le Kang, Zhongliang Li, Feixun Zhao and Chaoyin Xu

National Synchrotron Radiation Laboratory, University of Science and Technology of China, Hefei, Anhui, People's Republic of China. E-mail: phoenixf@mail.ustc.edu.cn

A scanning dynamically focusing sagittal X-ray monochromator accepting 3 mrad × 0.1 mrad from a 6 T wiggler has been designed for XAFS measurements. In the energy range 4.1–12.4 keV, the slope error of the second cylindrical crystal caused by anticlastic bending must be less than 1/5 of the Darwin width of the crystal or the photon flux will decrease drastically. Two methods to minimize the anticlastic bending are proposed. Thin crystals with stiffening ribs and thin crystals with an aspect ratio equal to the 'golden value' are evaluated by finite-element analysis and by long-trace-profiler characterization. Both approaches are satisfactory, but the 'golden value' approach is preferred in this case for the second crystal of the new monochromator not only because it is easy to manufacture but also because the surface is smoother than the ribbed crystal.

Keywords: sagittal focusing; anticlastic bending; stiffening ribs; golden value.

1. Introduction

The Hefei synchrotron is a second-generation synchrotron radiation light source operating at 0.8 GeV. Station U7B is dedicated to X-ray absorption spectroscopy (XAFS, EXAFS and XANES) in the energy range 4.1–12.4 keV. The station currently accepts 1 mrad × 0.1 mrad of the fan radiation from a 6 T superconducting single-period wiggler. The distance between the source and the sample is 12 m and the focusing spot on the sample is about 15 mm × 1 mm because there are no focusing optics in the beamline. In order to increase the intensity on the sample without changing the high-energy resolution (10^{-4}), we plan to replace the existing double-plane crystal monochromator with a sagittal-focusing monochromator that has larger horizontal acceptance and smaller spot size at the sample. Dynamically bent sagittal focusing optics in the 1/3 magnification are widely used for efficiently condensing X-ray beams with large divergence in one plane. Unfortunately the magnification factor cannot satisfy the optimal magnification factor of 1/3 (Sparks & Borie, 1980) and has to be set as 4.88:1 owing to space restrictions.

When a thin plate is bent in one direction it also becomes curved in a direction perpendicular to the first one; this is termed 'anticlastic bending'. The curvature has a negative sign in the meridional direction and its value depends on the sagittal radius, the elastic property of the material, the geometric parameters of the plate and the boundary conditions. The curvature results in a change in the incident angle of the incident radiation in the meridional plane. At some distance from the center of the second crystal, which is bent in the sagittal direction, the angle difference can exceed the Darwin width and the throughput of the monochromator will decrease drastically.

In this article we will describe the relative performances of crystals with stiffening ribs (Sparks & Ice, 1982) and crystals with a 'golden value' width-to-length aspect ratio (Kushnir et al., 1993). Both designs reduce anticlastic curvature of cylindrical bent crystals, and their relative performances are compared with long-trace-profiler (LTP) measurements and with finite-element-analysis (FEA) calculations.

2. Anticlastic distortion

A pure bending moment applied to a thin rectangular crystal plate (thickness $t \ll$ radius R_s) in the sagittal direction results in a negative-sign meridional curvature according to Hook's law (Fig. 1), which is termed 'anticlastic curvature', R_a. Anticlastic curvature is related to the fourth rank tensor of the elastic compliance and the sagittal radius R_s when the crystal is simply supported (Krisch et al., 1991), by

$$R_a = (s_{33}/s_{13})R_s. \tag{1}$$

With isotropic assumption, s_{13}/s_{33} is know as the Poisson ratio of the material.

The crystal may be fixed on one side or two sides, so the anticlastic curvature cannot achieve the minimum value of $(s_{33}/s_{13})R_s$ owing to the influence of the fixed edges. The following expression takes into account the influence of the fixed edges (Krisch et al., 1991),

$$\frac{(s_{13}/s_{33})R_a}{R_s} = 1 + \frac{2}{3}\left(1 + \frac{s_{13}}{s_{33}}\right)\frac{X^2}{Y^2}. \tag{2}$$
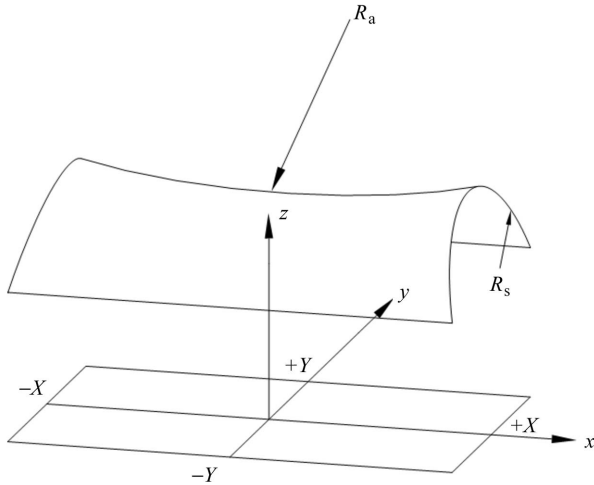
Figure 1
Geometry of the anticlastic bending affection.

If $X \ll Y$, the influence of the edges is neglected and the expression is given by (1).

Anticlastic bending will produce an error in the Bragg angle along the illuminated crystal, $\Delta\theta_E$, which increases with the vertical divergence of the synchrotron beam. The error for a small vertical divergence is given by

$$\Delta\theta_E = \frac{F_1 \varphi_v}{R_a \sin\theta_B}. \tag{3}$$

Here F_1 is the distance between the source and the bent crystal, φ_v is the vertical divergence of the synchrotron beam, R_a denotes the anticlastic curvature and θ_B is the Bragg angle. For $F_1 = 10$ m, magnification factor $M = 1:4.88$, $\varphi_v = 0.05$ mrad (the worst ray), Poisson ratio $\sigma = 0.262$ and effective crystal dimensions (not clamped) of 60 mm × 40 mm × 0.5 mm, $\Delta\theta_E$ as a function of photon energy is calculated and shown in Fig. 2. The LTP measurement and FEA results of the slope error along the central 10 mm in the meridional direction are compared in Fig. 3.

3. Methods for reducing the anticlastic bending

3.1. Crystals with ribs

To reduce the anticlastic curvature, ribs transverse to the bending curvature were attached to the back surface of the crystal with various glues. These ribs significantly reduce the anticlastic bending without seriously stiffening the crystal in the direction of the desired bending radius. The relationship between the bending radius R_s and the resulting anticlastic radius R_a for a ribbed crystal can be shown as

$$R_a/R_s \simeq -\frac{1}{\sigma}\left[1 + \frac{w}{s}\left(\frac{h}{t}\right)^3(1-\sigma^2)\right]. \tag{4}$$

The parameters are shown in Fig. 4. In our experiment, 11 ribs are glued onto a thin rectangular crystal, which allows for more than 80% transmission compared with two parallel plane crystals (Artemev et al., 2001). In fact, the approximation
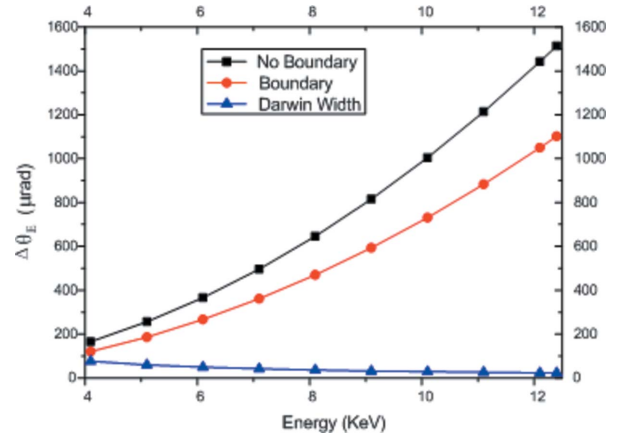
Figure 2
$\Delta\theta_E$ as a function of energy for boundary and no boundary conditions.
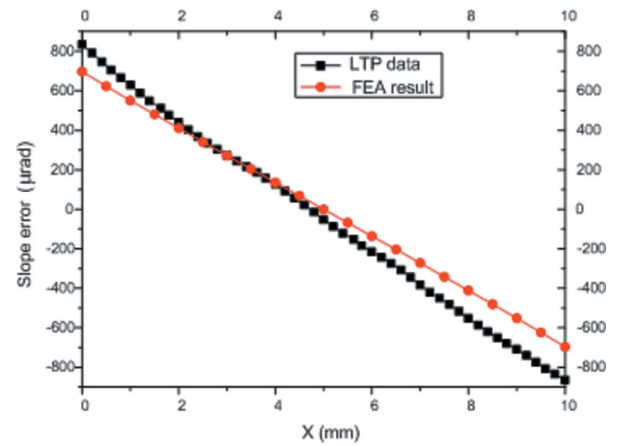
Figure 3
Slope error caused by anticlastic bending along the meridional direction (X) ($R_s = 1$ m).

above does not give an accurate value of the bending radius because the bending radius oscillates widely under the ribs (Hazemann et al., 1995) (Fig. 5a). However, we can still choose parameters of the crystal based on the formulation that R_a/R_s should be bigger than 2000 to make $\Delta\theta_E$ less than 1/5 of the Darwin width.

The geometric parameters of the ribbed crystal are $w = 0.5$ mm, $s = 3$ mm, $t = 0.5$ mm and $h = 12$ mm. Fig. 5(b) shows the FEA result and LTP measurement data.

Although anticlastic bending can be suppressed to less than 4 µrad in the central 10 mm in the meridional direction with ribbed crystals, there are still some disadvantages to this approach. The sagittal curvature oscillates periodically according to the distribution of the ribs, and these waves
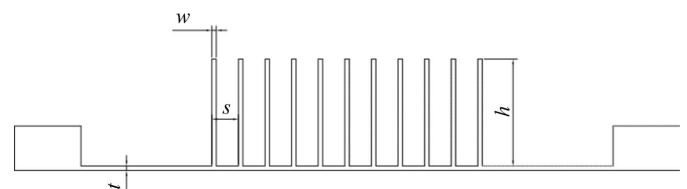
Figure 4
Schematic diagram of the ribbed crystal.
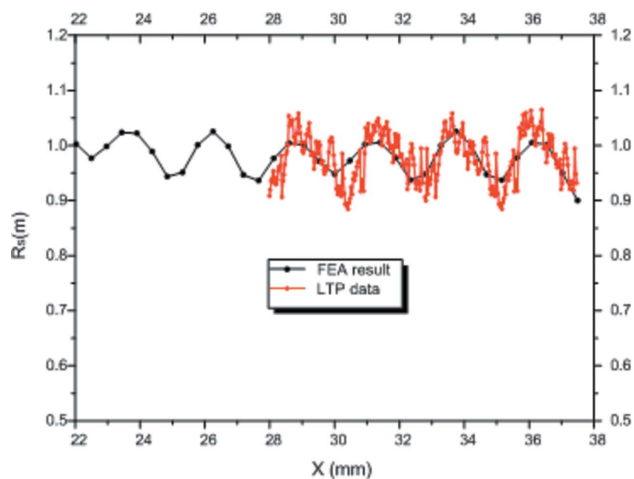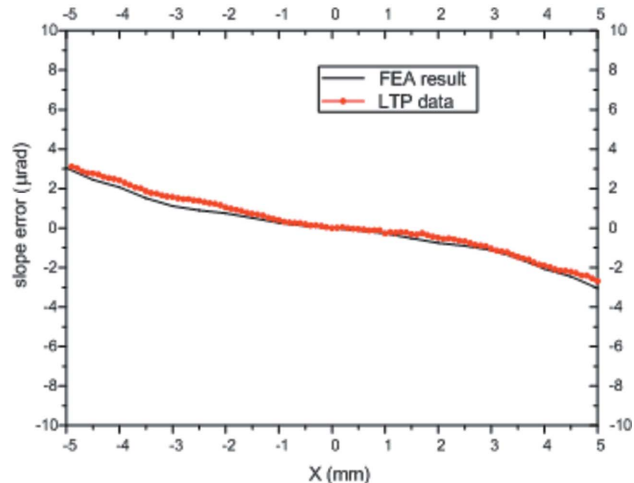
Figure 5
(a) The curvature of the ribbed crystal along the sagittal direction (Y) (R_s = 1 m). (b) Slope error caused by anticlastic bending along the meridional direction (X) (R_s = 1 m).

prevent the diffraction from propagating on the whole reflective surface of the crystal. However, the distortion of the crystal lattice is small in the present energy range (4.1–12.4 keV) (Schulze et al., 1998). To avoid these disadvantages, there is another method for minimizing the anticlastic bending, called the 'golden value' ratio.

3.2. Crystals with the 'golden value' ratio

Anticlastic curvature is a function of the crystal aspect ratio ($\gamma = X/Y$, Fig. 1) and becomes zero in the middle of the crystal at an aspect ratio dependent on the Poisson ratio. Within the thin-crystal approximation, and near particular aspect ratios, there is an extended central zone with slope errors less than the Darwin width of the crystal. With simply supported crystals, this ratio is 2.360 or larger than 6.6 (Bilsborrow et al., 2006) for $\sigma = 0.262$. Under clamped conditions (our experimental bender) this ratio reduces to 1.42 owing to the influence of the clamped edge.
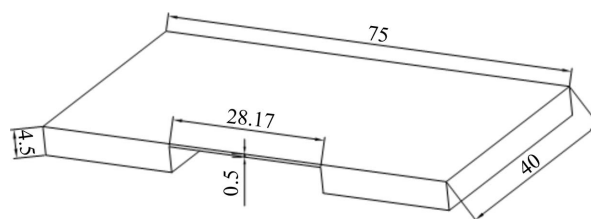
Figure 6
Schematic diagram of the test crystal. Dimensions in mm.
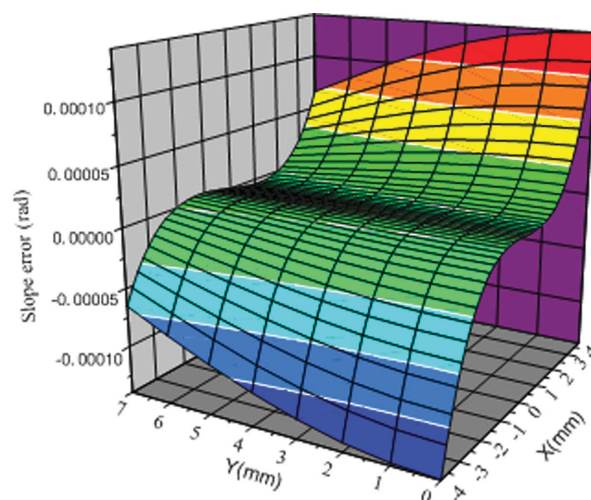
Figure 7
Slope error caused by anticlastic bending in the meridional direction (X) on the crystal surface from the center ($Y = 0$) to the edge ($Y = 7$) (R_s = 1 m).

The test crystal for LTP measurement is shown schematically in Fig. 6. The effective area is 40 mm × 28.17 mm. We found that the slope error in the meridional direction on the crystal surface becomes smaller from the center to the edge by FEA (Fig. 7). So we just need to know the slope error on the symmetry line ($Y = 0$ on Fig. 7) of the crystal surface in the meridonal direction (Fig. 8).

For our case the maximal length of the footprint on the cylindrical bent crystal is $10(0.1/\sin 9.18) = 6.27$ mm, the
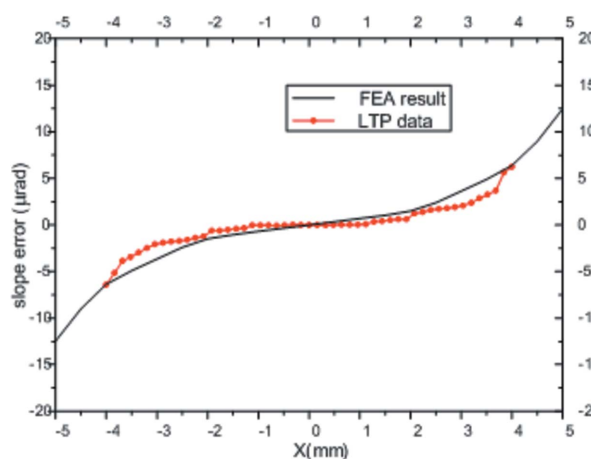
Figure 8
Slope error caused by anticlastic bending on the symmetry line in the meridional direction (X) (R_s = 1 m).

maximal slope error is 3 µrad according to the LTP data, which is much smaller than the Darwin width; however, it exceeds 12 µrad in 10 mm and increases faster at the edge. For other beamlines with longer distances between the source and the monochromator, or higher energy, the longer footprint means larger slope error and it may exceed the Darwin width of the crystal. Some beamlines need the sagittal focusing monochromator to collect larger horizontal divergence X-rays, but this means that the second crystal will become much longer to satisfy the golden-value ratio, and this is restricted by the narrow space in the vacuum chamber.

4. Conclusion

This evaluation permitted us to find an optimum solution to minimize the anticlastic bending to an acceptable level within the energy range 4.1–12.4 keV at a magnification of 1/3. The stiffening ribs perform very well in minimizing the anticlastic bending, *i.e.* the slope error caused by anticlastic bending does not exceed 5 µrad on the whole diffraction surface at R_s = 1 m, but the oscillation of the sagittal curvature may decrease the throughput of the monochromator, and the crystal is difficult to manufacture. The crystal with the golden-value ratio decreases the anticlastic bending greatly, but the anticlastic curvature is still not small enough compared with the Darwin width of the crystal with footprint longer than 10 mm especially at high energy. The golden-value ratio of $\gamma = X/Y$ increases the useless length in the meridional direction, causing difficulties in designing the bending mechanism and the rotation stage of the dynamically scanning sagittal-focusing monochromator. However, we are still inclined to choose the golden-value crystal as the second crystal of our new monochromator because it is easy to manufacture and the surface is much smoother compared with the ribbed crystal for obtaining a higher photon density. We are still testing other types of crystals such as the two-ribbed crystal (Tajiri *et al.*, 2001) and the slotted crystal (Mills *et al.*, 1986) to find a commercial and suitable style for our sagittal focusing monochromator.

References

Artemev, A., Artemiev, N., Busetto, E., Hrdy, J., Mrazek, D. & Savoia, A. (2001). *Nucl. Instrum. Methods Phys. Res. A*, **467–468**, 373–376.
Bilsborrow, R. L., Atkinson, P. A., Bliss, N., Dent, A. J., Dobson, B. R. & Stephenson, P. C. (2006). *J. Synchrotron Rad.* **13**, 54–58.
Hazemann, J. L., Nayouf, K. & de Bergevin, F. (1995). *Nucl. Instrum. Methods Phys. Res. B*, **97**, 547–550.
Krisch, M., Freund, A., Marot, G. & Zhang, L. (1991). *Nucl. Instrum. Methods Phys. Res. A*, **305**, 208–213.
Kushnir, V. I., Quintana, J. P. & Georgopoulos, P. (1993). *Nucl. Instrum. Methods Phys. Res. A*, **328**, 588–591.
Mills, D. M., Henderson, C. & Batterman, B. W. (1986). *Nucl. Instrum. Methods Phys. Res. A*, **246**, 356–359.
Schulze, C., Lienert, U., Hanfland, M., Lorenzen, M. & Zontone, F. (1998). *J. Synchrotron Rad.* **5**, 77–81.
Sparks, C. J. Jr & Borie, B. S. (1980). *Nucl. Instrum. Methods*, **172**, 237–242.
Sparks, C. J. Jr & Ice, G. E. (1982). *Nucl. Instrum. Methods*, **194**, 73–78.
Tajiri, G., Khounsary, A. & Mancini, D. (2001). (2001). *Proc. SPIE*, **4145**, 114–121.